ELSEVIER

Surface Science 492 (2001) 41–54

SURFACE SCIENCE

www.elsevier.com/locate/susc

Oxygen-induced stress-modified reconstructions of the Ta(1 1 0)/Al_2O_3(1 1 −2 0) surface: a surface X-ray diffraction study

O. Robach [a,b,*], I.K. Robinson [b], C.S. Durfee [b], B.W. Wiemeyer [b], C.P. Flynn [b]

[a] *ESRF, BP 220, F-38043 Grenoble Cedex, France*

[b] *Department of Physics, University of Illinois at Urbana-Champaign, Urbana, IL 61801, USA*

Received 25 January 2001; accepted for publication 22 June 2001

Abstract

The knowledge of the surface structure of thick metallic buffer layers is important to understand subsequent growth. We present here a surface X-ray diffraction study of an oxygen-induced surface reconstruction observed on thick Ta(1 1 0) layers grown on sapphire (1 1 −2 0). The solving of the atomic structure was performed using both Ta crystal truncation rods and superstructure rods. The model found for the reconstruction can be described as a misfit defect network at the interface between one plane of TaO(1 1 1) in Kurdjumov–Sachs epitaxy and the Ta. The reconstruction is not always commensurate. This probably arises from the coexistence of several commensurate supercells of slightly different periods. A small anisotropy (0.1–0.2%) of the in-plane lattice parameter of the Ta has been measured in all the samples. This anisotropy, which is due to the epitaxy on the sapphire, induces on the surface a selection of one of the two domains of the reconstruction. © 2001 Elsevier Science B.V. All rights reserved.

Keywords: Tantalum; Oxidation; Aluminum oxide; X-ray scattering, diffraction, and reflection; Surface structure, morphology, roughness, and topography; Surface relaxation and reconstruction; Surface stress; Metallic films

1. Introduction

Thick metallic buffer layers on oxide substrates (Al_2O_3, MgO) are commonly used as substrates for the molecular beam epitaxy (MBE) growth of other materials such as metals or superconductors. The use of buffer layers often represents an attractive alternative to the use of metallic single crystals, since they yield better flatness and better crystalline quality of the surface. Buffer layers of Ta and Nb on Al_2O_3(1 1 −2 0) have the additional interest of being ''single crystalline'', i.e. they grow with only one orientation.

Knowing the atomic structure of the surface of the buffer layer is an important starting point to understand the mechanisms governing the subsequent growth of the adsorbate. Ta buffer layers grown on sapphire at a substrate temperature of 900°C have been found to exhibit a reconstruction which is most likely induced by oxygen desorbing from the alumina at this high temperature. The structure of this reconstruction is influenced by the

* Corresponding author. Address: ESRF, BP 220, F-38043 Grenoble Cedex, France. Tel.: +33-4-76-88-21-62/25-99; fax: +33-4-76-88-21-60.

E-mail address: robach@esrf.fr (O. Robach).

0039-6028/01/$ - see front matter © 2001 Elsevier Science B.V. All rights reserved.
PII: S0039-6028(01)01394-2

epitaxial strains induced in the Ta by the Al_2O_3, as evidenced by the observation of only one of the two possible domains of the reconstruction. It also appears to depend strongly on the growth conditions and on the Ta layer thickness.

Here we report an investigation of this reconstruction by surface X-ray diffraction (SXRD) and propose a model for the atomic structure. X-ray data concerning the dependence on the Ta thickness of the positions of the reconstruction peaks and of the residual strains in the Ta are also reported.

One important remark is that, since Nb and Ta have practically the same crystallographic structure (BCC, $a_{Ta} = 3.3058$ Å, $a_{Nb} = 3.3066$ Å [1] at 300 K), the results of the present study on Ta are expected to apply as well to Nb. A reconstruction with a very similar pattern has already been reported for Nb layers on Al_2O_3 [2], and also for Nb(1 1 0) single crystals contaminated by oxygen, [3] but its atomic structure is yet unsolved.

After a few considerations about the epitaxy of Ta on Al_2O_3 (Section 2.1), the experimental setup will be described in Section 2.2. Results will then be presented, starting with the solving of the atomic structure of the reconstruction on one particular sample (Section 3.1), and continuing with the results about the film thickness dependence of the reconstruction (Section 3.2). The results will be discussed in Section 4, followed by the conclusion.

2. Experiments

2.1. Epitaxy of Ta(1 1 0) on Al_2O_3(1 1 −2 0)

As niobium, tantalum (BCC structure) grows on sapphire (1 1 −2 0) (corundum structure) with the epitaxial relationship [4]:

$$\begin{cases} (1\,1\,0)_{\mathrm{Ta}} \| (1\,1\,\bar{2}\,0)_{\mathrm{Al_2O_3}} \\ [1\,\bar{1}\,1]_{\mathrm{Ta}} \| [0\,0\,0\,1]_{\mathrm{Al_2O_3}} \end{cases}$$

Fig. 1 shows an in-plane view of this epitaxial relationship, together with a schematics of the (1 × 1) unit cell of the Ta(1 1 0) surface. Another way to describe the epitaxy is to say that Ta grows

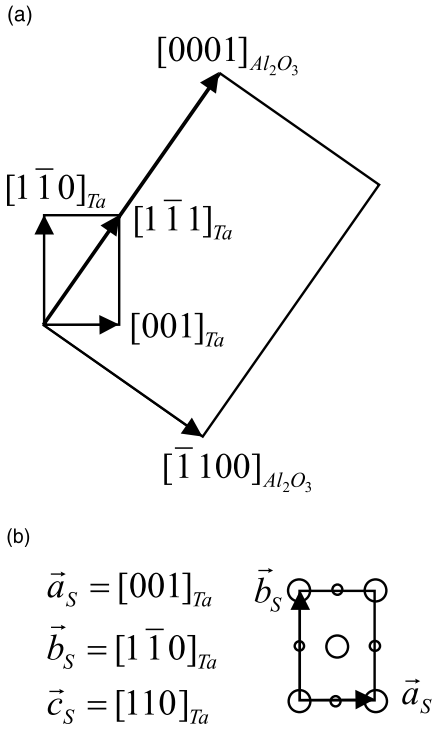

Fig. 1. (a) Epitaxial relationship between Ta(1 1 0) and Al_2O_3-(1 1 −2 0). (b) (1 × 1) Surface unit cell used to define the Miller indexes ($H\,K\,L$). Big circles: Atoms at $z = 0$, small circles: atoms at $z = 0.5$.

so as to extend the almost-BCC lattice of the aluminum ions in the sapphire. This epitaxial relationship yields only one orientation in the Ta, which makes the system very attractive to produce a "single crystal" buffer layer of Ta. At the interface between Ta and Al_2O_3, the lattice mismatch is $\frac{}{}$11.86% along the sapphire [0 0 0 1] axis ($2||\vec{a}_S + \vec{b}_S||_{Ta}/c_{Al_2O_3} = 0.8814$) and $\underline{}$−1.76% along the sapphire [1 −1 0] axis ($||2\vec{a}_S - \vec{b}_S||_{Ta}/a_{S\text{–}Al_2O_3} = 0.9824$).

One important remark is that the epitaxy on Al_2O_3 renders the Ta anisotropic from the point of view of the epitaxial strains: the $[1\,{-1}\,1]_{\text{Ta-bulk}}$ direction is no longer equivalent to the $[1\,1\,1]_{\text{Ta-bulk}}$ direction.

By analogy with the Nb/Al_2O_3 interface, which has been extensively studied by TEM by Gutekunst et al. [5,6], the Ta/Al_2O_3 interface is expected to have its epitaxial stresses relaxed through

a misfit dislocation network. The residual strains in the Ta after this relaxation will depend on the dislocation network present at the interface.

2.2. Experimental setup

The SXRD experiments were performed at the UIUC Materials Research Laboratory (Urbana, Illinois) in the "Epicenter", which is an ensemble of vacuum chambers connected to each other by UHV transfer tubes [7]. The samples were grown in a Perkin–Elmer 430 MBE chamber dedicated to the growth of refractory metals, then studied by RHEED in this chamber, and finally transferred under vacuum into the "diffraction chamber" where they were studied by in situ SXRD. The diffraction chamber has a base pressure of 6×10^{-10} Torr, is equipped with a beryllium window for the passage of X-rays, and is mounted on a five-circles diffractometer. The X-ray source is a Cu rotating anode, with a pyrolytic graphite monochromator to focus the beam vertically (the sample being horizontal). Further details about the diffraction station can be found in Ref. [8].

The Ta films were grown on epitaxial grade sapphire $(-1\ -1\ 2\ 0)$ substrates (0.02 in. thick, epi-polish finish, Alfa Aesar) by e-beam evaporation of a Ta charge of 99.98% purity (Alfa Aesar), with a growth rate of 0.4 Å/s (or 0.2 Å/s), and a substrate temperature of 900°C, as measured by an optical pyrometer on the Mo sample holder.

The conditions for the X-ray measurements were the following: the beam had a spot size at the sample of 3 mm (H) × 5 mm (V), and a divergence of 1.3° (V) × 0.3° (H). For the measurements of the Ta crystal truncation rods (CTRs), the detector had an acceptance of 1.3° (V) × 0.3° (H) and 15 mm (V) × 6 mm (H), the horizontal divergence being fixed by Sollers slits. For the measurements of the reconstruction peaks, it was necessary to use a collimator (two 2 mm wide horizontal slits at 300 and 600 mm from the sample) to avoid seeing the edges of the sample.

Ex situ residual strains measurements in the Ta were performed on beamline X16C of the National Synchrotron Light Source at Brookhaven National Laboratory (Upton, New York), using a kappa diffractometer in the four-circles symmetric mode, with a Si(1 1 1) analyser crystal in front of the detector. Neighboring sapphire peaks were used as a reference for measuring the momentum transfer of the Ta Bragg peaks.

Additional residual strains measurements were performed at the Materials Research Laboratory (Urbana) using a Phillips X'pert diffractometer. The setup of the X'Pert diffractometer is the same as the one of the Phillips Materials Research Diffractometer [9], except for the addition of a parabolic mirror in the primary optics.

The results we present here concern four samples. The first sample was 1000 Å thick. It was on this sample that the asymmetric reconstruction of the Ta(1 1 0) surface, previously only observed by RHEED, was first clearly identified by SXRD. This sample was the subject of an in-depth analysis of the diffraction features, the CTRs ([10,11]) and the reconstruction peaks, in view of solving the atomic structure of the reconstruction.

The other three samples were respectively 300, 1000, and 3800 Å thick. They were grown in view of trying to reveal a possible link between the reconstruction of the Ta surface and the degree of relaxation of the Ta.

3. Results

3.1. Atomic structure

3.1.1. Description of the diffraction pattern

For the purpose of finding the atomic structure, we will consider here only one sample, on which a (5×7) reconstruction was observed. It is important to note that the multiplicity of the reconstruction is not always (5×7) but varies from sample to sample. The physical tendencies deduced by solving the (5×7) should however be correct, because the reconstruction pattern is very similar for all the samples.

This sample was 1000 Å thick and was grown with a deposition rate of 0.2 Å/s. We performed quantitative intensity measurements of the reconstruction peaks, of the reconstruction rods, and of the Ta CTRs. We then searched for a model which would reproduce all those data simultaneously.

The reconstruction peaks were first located by a big mesh scan in H and K at $L = 0.3$, that covered approximately one half of the reciprocal plane (H and K between 0.5 and 2.0). This mesh scan (not shown) revealed first that there were very few non-extinct superstructure peaks, and secondly that all the superstructure peaks were located in the vicinity of the Ta CTRs.

The pattern obtained by X-ray diffraction was consistent with the one obtained by RHEED in the growth chamber, except for a much smaller number of peaks. The number of peaks was also smaller than on the LEED patterns published by Swiech et al. [2], for a similar reconstruction of Nb/Al_2O_3. This reflects the fact that many of the numerous multiple diffraction peaks present in electron diffraction are absent in X-ray diffraction.

Quantitative measurements of the superstructure peaks intensities at $L = 0.3$ were performed by doing rocking scans around the (5×7) positions. The resulting structure factors $|F_{HK}|$ are represented in Fig. 2, as a function of H and K, by half circles of radius proportional to $|F_{HK}|$. Only one half of the reciprocal space has been represented.

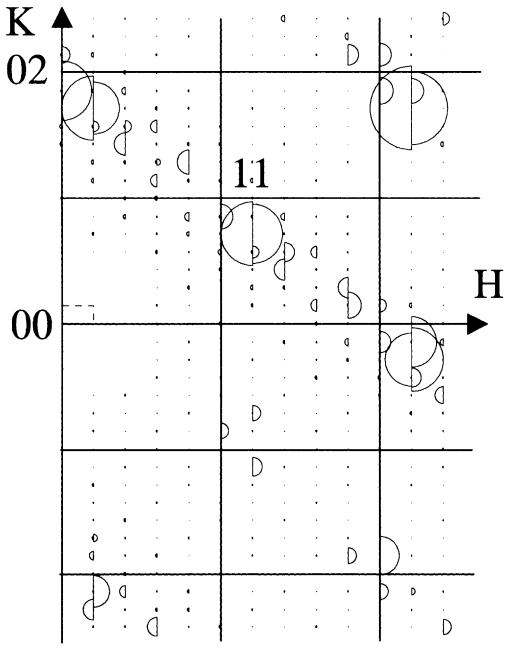

Fig. 2. Comparison between the experimental (right side) and calculated (left side) in-plane structure factors of the (5×7) reconstruction. Fit with the "KS" model. Only the fractional order points are plotted.

A feature visible in Fig. 2 is the asymmetry of the reconstruction: there is an intense superstructure peak at $(1 + 1/5, 1 - 2/7)$ but there is almost no intensity at $(1 + 1/5, -1 + 2/7)$, meaning that the symmetry is at most P2, and not P2mm as for the unreconstructed Ta(1 1 0) surface. As will be seen in Section 4, this asymmetry is the result of the anisotropic in-plane strain induced in the Ta by the alumina.

The pattern of Fig. 2 shows three other important features: first, the $(1\,1\,L)$, $(2\,0\,L)$, $(0\,2\,L)$ and $(2\,2\,L)$ rods all have a strong superstructure peak separated by $(\Delta H; \Delta K) = (1/5 - 2/7)$ from the integer rod, but the $(1\,-1\,L)$ and $(2\,-2\,L)$ rods do not have this superstructure peak. Secondly the superstructure peaks are grouped preferentially along the lines going through the integer rods and parallel to the $H = -K$ line. Thirdly, the superstructure peak environment is very asymmetric around the integer rods: there is a very intense superstructure peak at $(\Delta H; \Delta K) = (+1/5, -2/7)$ but no superstructure peak at $(-1/5, +2/7)$. As will be seen later, these three tendencies are characteristic of a structure involving a shear of the Ta lattice along the $[1\,-1\,1]_{\text{Ta-bulk}}$ direction.

In order to determine if the observed pattern came from a rather "two-dimensional (2D)" object, like a surface reconstruction, or from a rather "three-dimensional (3D)" object, like a misfit dislocation network, the superstructure peak intensities were measured at different L's. The superstructure rods were found to have a quite flat profile in L, indicating that the reconstruction was limited to a few atomic planes near the surface. Linear scans in H and K performed at different values of L showed that the superstructure rods were parallel to the Ta CTRs. This excluded facetting as a possible origin of the observed pattern.

The data set was completed by measuring quantitatively the intensities of the Ta CTRs. The structure factors along the CTRs are plotted versus L in Fig. 3, after averaging the data with a P2 symmetry. The break of the P2mm symmetry observed in the reconstruction pattern is also visible on the truncation rods: the $(H\,K\,L)$ rod is no longer equivalent to the $(H\,-K\,L)$ rod.

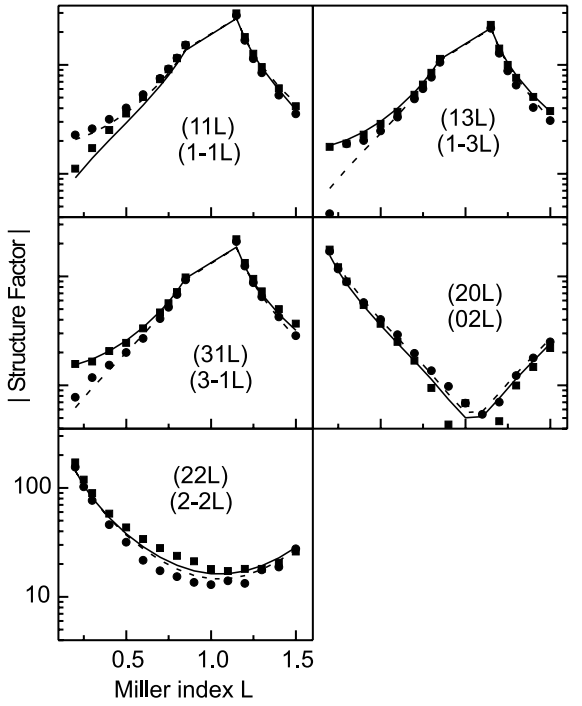

Fig. 3. Comparison between the experimental and calculated structure factors along the Ta CTRs. The calculated points correspond to a fit with the (5×7) "KS" model of Fig. 5b. Rods with $K > 0$ and $(20L)$: calc. (—), exp. (■). Rods with $K < 0$ and $(02L)$: calc. (- - -), exp. (●).

One interest of measuring the Ta CTRs was that we could use them to narrow the range of possible models for the (5×7) reconstruction. Indeed, the CTRs are an image of the scattering by the "average" (1×1) cell, i.e. the cell obtained by averaging the electronic density over the 35 (1×1) cells forming the (5×7) supercell. The fitting of the CTRs can therefore be done with a (1×1) model, which is much simpler to manipulate than a (5×7) model. In addition, the Ta CTRs provided a measurement of the surface roughness.

3.1.2. Solving of the atomic structure

3.1.2.1. Introduction. Since the solving of a structure involving so many atoms is not straightforward, we will describe here some of the critical steps that were taken in solving it, before presenting the final model. This solving made extensive use of the ROD program initially developed by Vlieg [12,13].

The diffraction pattern of the (5×7) reconstruction (including the CTRs) shows only a P2 symmetry (i.e. $|F_{HKL}| = |F_{-H-KL}|$) meaning that the (5×7) supercell is either (1) P2 or (2) P1 with two domains rotated by 180°. Since from the point of view of diffraction these two cases are almost indistinguishable, it does not reduce the generality of the problem to assume a P2 symmetry. Assuming now that only the last Ta plane of the (5×7) supercell is reconstructed (which is justified by the rather flat profile of the reconstruction rods along L), the P2 symmetry reduces the number of independent structural parameters to $70/2 = 35$ atoms times four parameters per atom $(\mathrm{d}x, \mathrm{d}y, \mathrm{d}z + \text{occupancy})$, giving a total of 140 parameters. This was clearly a too large number to hope that a fitting procedure starting from the bulk positions would be able to converge. It was therefore necessary to find "by hand" an approximate model of the structure, before refining the structural parameters of the model by a fit of the diffracted intensities.

3.1.2.2. Fit of the Ta crystal truncation rods. The first step was to find a model for the (1×1) cell that would reproduce the profiles in L of the Ta CTRs. This was done first qualitatively: we examined the intensity at the anti-Bragg points of the different (HKL) CTRs (Fig. 3), and classified those points as "high intensity" or "low intensity" as a function of H and K, in order to obtain "extinction rules". We then tried to find where in (x, y) a new Ta atom should be added in the (1×1) cell so that the term:

$$1 + \cos(2\pi(Hx + Ky))$$

would give the correct extinction rules. By applying this very qualitative method, we found that adding atoms shifted by $(\Delta x, \Delta y) = (1/4, 1/4)$ from the bulk positions enabled to decrease the χ^2 significantly. The χ^2 decreased from 4.2 for a model with all atoms at the bulk positions and a last-plane occupancy of 0.68, to 1.50 for a model with atoms at the bulk positions (occupancy 0.62) and atoms shifted by $(1/4, 1/4)$ (occupancy 0.25).

This suggested, as a first approximation of the (5×7) supercell, a one-plane model in which 62% of the 70 atoms (27 atoms) are at their bulk (x, y)

positions, 25% (17–18 atoms) are shifted from the bulk positions by $(1/4, 1/4)$, and 13% (nine atoms) are missing. Of course at this stage we had no indication about how the displaced atoms are distributed among the 35 (1×1) cells contained in the (5×7) supercell.

This simple model gives extinction rules that are correct for all the rods except the {2 2} CTRs: the calculation gives $I(2\,2) = I(2\,-2)$ while experimentally $I(2\,2) > I(2\,-2)$. Further improvement of the fit (χ^2 of 1.25) could be obtained by adding to the model other Ta atoms shifted by a different $(\Delta x, \Delta y, \Delta z)$, but the solution was not unique. Among those models, the ones involving atoms displaced in z seemed the most relevant because they enabled to reproduce the slight undulation observed on the $(2\,0\,L)$ and $(0\,2\,L)$ CTRs.

This analysis of the CTRs provided the very useful information that the main feature of the structure was a shear of the Ta lattice along the $x = y$ direction of the (1×1) cell, i.e. along the $[1\,-1\,1]_{\mathrm{Ta}}$ direction (parallel to the sapphire c axis). This seemed reasonable since the $[1\,-1\,1]$ is a direction of easy shear in BCC metals: faults in the stacking of the $[-1\,1\,2]$ planes corresponding to a slip along the $[1\,-1\,1]$ direction are a very common defect in these metals [14].

Note that we completely neglected the Ta/sapphire interface in the calculation of the CTRs, because the film thickness is two times larger than the penetration depth of the X-rays.

3.1.2.3. Fit of the (5×7) reconstruction. The next step was to find how the displaced atoms should be distributed over the 35 (1×1) cells of the (5×7) supercell to get a reconstruction pattern matching the experimental one (Fig. 2).

A very useful hint for the correct structure was provided by the study of Pantel et al. [3] about the oxidation of Nb. This study was performed on the (1 1 0) surface of a Nb single crystal. The authors observed by LEED a structure very similar to the (5×7), which occurred at an intermediate stage of the surface preparation. Auger analysis of this structure (in Ref. [3]) showed 0.2–0.4 monolayer of oxygen. A model was proposed, which involved a layer of NbO(1 1 1) coinciding periodically with the Nb(1 1 0) so as to create the supercell of the reconstruction. However, the in-plane orientation of the NbO proposed in this study (Fig. 9 of Ref. [3]) did not fit with the positions of the Bragg peaks attributed to NbO.

Other authors also obtained TaO(1 1 1) or NbO(1 1 1) as the first product of the dry oxidation in studies of the interaction of oxygen with the surface of Ta(1 1 0) [15,16] and Nb(1 1 0) [17,18] single crystals, and with the surface of Nb(1 1 0) grown on Al_2O_3 [19]. It should be noted however that the observation of TaO(1 1 1) is not systematic: several other oxygen-induced reconstructions were obtained on Ta(1 1 0) and Nb(1 1 0) single crystals [20], and on Nb(1 1 0) films grown on Al_2O_3 [21].

Following the conclusions of Pantel et al. [3], we focussed on models involving a layer of TaO(1 1 1) at the surface of Ta(1 1 0). In our modeling, we ignore the oxygen atoms entirely because we could not disentangle their effect on the diffracted intensities from the effect of small displacements of the Ta atoms.

From Refs. [15,16], the TaO (NaCl structure, $a = 4.439$ Å) grows with the $[1\,1\,-2]$ TaO direction aligned with the $[1\,-1\,0]$ Ta direction (Nishiyama–Wassermann (NW) orientation). This epitaxial relationship is represented in Fig. 4a. It gives a fairly large lattice mismatch along the $[1\,-1\,0]$ Ta direc-

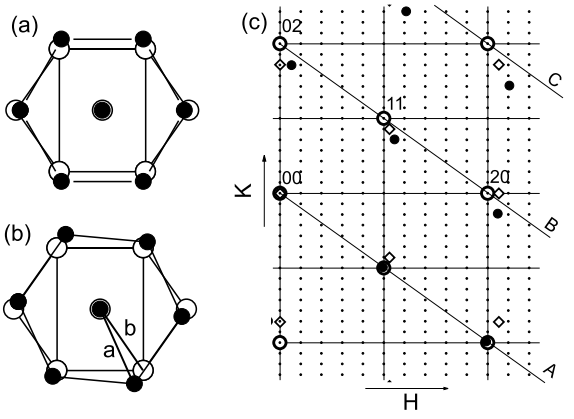

Fig. 4. The NW (a) and KS (b) epitaxy of TaO(1 1 1) (●) on Ta(1 1 0) (○). Only the Ta atoms of TaO are represented. a and b are the nearest-neighbor distances in TaO and Ta, respectively. (c) 2D in-plane reciprocal lattice for Ta(1 1 0) (○), TaO(1 1 1) in KS epitaxy (●) and TaO(1 1 1) in NW epitaxy (◇). The (5×7) lattice is indicated by small dots.

tion, +16%, and a smaller mismatch, −5.4%, along the [1 0 0] direction. Using the criterion given in Ref. [22], the value of 1.096 of the a/b ratio (see Fig. 4b for the definition of a and b) should make the Kurdjumov–Sachs (KS) epitaxy energetically more favorable. This second epitaxial relationship, in which the $[1\,-1\,1]$ Ta direction is aligned with the $[-1\,0\,1]$ TaO direction, is represented in Fig. 4b. It gives almost no mismatch along the $[-1\,1\,2]$ Ta direction (+0.71%) (considering the spacing of the atomic rows parallel to $[1\,-1\,1]_{\mathrm{Ta}}$), and a +9.64% mismatch along the $[1\,-1\,1]$ Ta direction.

The relative in-plane positions of the Ta CTRs and TaO diffraction rods are represented in Fig. 4c for TaO(1 1 1) in NW and KS epitaxy.

For the KS epitaxy (Fig. 4c), the TaO rods are almost perfectly superimposed with the Ta CTRs along the $K = -H$ line ("A" line in Fig. 4c). Around the Ta CTRs belonging to the $K = 2 - H$ line ("B" line in Fig. 4c) (such as $(1\,1\,L)$, $(0\,2\,L)$, $(2\,0\,L)$), the TaO rods are very close to the main superstructure peak of the (5×7) reconstruction: they are located at $(H, K) = (H_{\mathrm{CTR}} + 0.11,\ K_{\mathrm{CTR}} - 0.28)$ while the reconstruction superstructure peaks are at $(H_{\mathrm{CTR}} + 1/5, K_{\mathrm{CTR}} - 2/7)$.

It is possible to make the TaO rods along the "B" line exactly match the superstructure peaks, provided that one applies a slight shear along $[1\,-1\,1]_{\mathrm{Ta}}$ to the TaO unit cell. By construction, the pseudo-hexagonal KS TaO obtained in this way gives Bragg peaks at $(1\,-1\,0)_{\mathrm{Ta}}$ and $(6/5\ 5/7\ 0)_{\mathrm{Ta}}$. However, it does not give the right peak position around the (2 2) Ta CTR: the peak of the TaO is two times too far away from the CTR, at $(2 + 2/5, 2 - 4/7)$ instead of $(2 + 1/5, 2 - 2/7)$. A pseudo-hexagonal layer of KS TaO on top of the Ta is therefore not sufficient to reproduce the (5×7) pattern.

Fig. 5a shows the superposition of the pseudo-hexagonal KS TaO layer with the Ta lattice, in the (5×7) supercell. Because this TaO is designed to have Bragg peaks superimposed with peaks of the (5×7), the atomic positions in the TaO coincide with the Ta sites at the corners of the (5×7) supercell. From Fig. 5a it is clear that there are regions of "good match" between the TaO and Ta lattices, as well as regions of "bad match". One can then wonder if trying to improve the match between the two lattices could be a way of getting the right diffraction pattern.

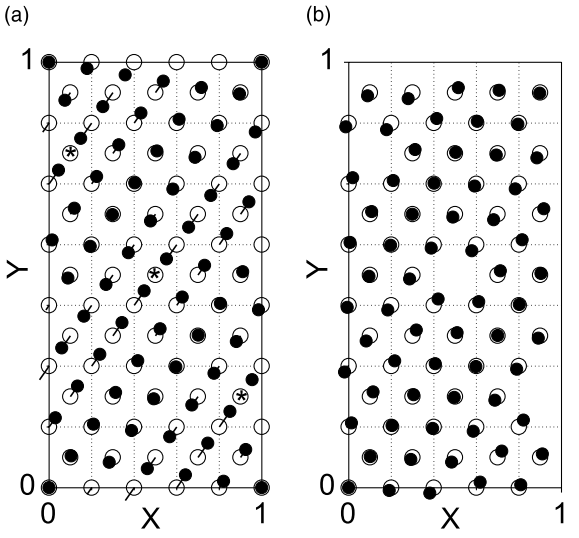

Fig. 5. (a) Superposition of the Ta(1 1 0) lattice (○) and of the pseudo-hexagonal KS TaO(1 1 1) lattice (●), in the (5×7) supercell. Only the Ta atoms of the TaO are represented. The "KS" model consists in moving collectively the "TaO" atoms towards the nearest Ta sites, to improve the matching between the two lattices. The collective motion is described by a parameter d_1, which is the percentage of the "TaO–Ta" distance (small segments in Fig. 5a) traveled by the TaO atoms. The (∗) signs show the Ta sites where a "misfit dislocation" will occur along the $[1\,-1\,1]_{\mathrm{Ta}}$ direction. (b) The best-fit (5×7) supercell ("KS" model with $d_1 = 0.57$).

This leads to displace the atoms of the TaO to improve their matching with the Ta lattice. The most direct way is to displace each Ta of the TaO towards the nearest site in the Ta, with an amplitude proportional to the distance to the site. This is equivalent to putting the atom of the TaO in a parabolic potential well centered on the nearest Ta site. One needs of course to avoid having two TaO atoms moving toward the same Ta site: the (∗) signs in Fig. 5a show the sites for which there is a collision problem. The "links" between the atoms of the TaO and the nearest Ta site are materialized by short segments in Fig. 5a.

This procedure creates a model which is a sort of misfit defect network at the interface between the pseudo-hexagonal KS TaO and the Ta. Along the atomic rows parallel to $[1\,-1\,1]_{\mathrm{Ta}}$, the structure is

equivalent to a one-dimensional (1D) misfit dislocation network, with one missing TaO atom each 23 sites of the Ta. Perpendicular to these rows, there is a perfect lattice match between the substrate and the overlayer (we neglected the +0.71% misfit between the KS TaO and the Ta along the $[-1\,1\,2]_{Ta}$ direction).

Coming back to a description of the model in terms of displacements of the last-plane Ta atoms from their bulk positions, one can remark that the model described in Fig. 5a involves only displacements of the Ta atoms along the $[1\,-1\,1]_{Ta}$ direction. This is consistent with the direction of atomic displacements that was expected from the analysis of the CTRs (Section 3.1.2.2).

We note d_1 the parameter describing the collective displacement of the Ta atoms of the TaO towards the Ta sites. The value $d_1 = 0$ corresponds to the simple pseudo-hexagonal KS TaO layer. The value $d_1 = 1$ corresponds to a layer of bulk Ta, with three atoms missing.

d_1 and the occupancy of the 67 Ta atoms of the TaO (occ_1) were adjusted by a fit of the experimental intensities. The data set consisted in 150 CTR points, 408 fractional-order points at $L = 0.3$ (204 measured with rocking scans, the other 204 ones being manually put to zero from the mesh scans), plus 90 points on the rods of the most intense fractional order points. The fitting parameters were, in addition to d_1 and occ_1, an overall scale factor S, the roughness β, the L-shift [13] (used only for the CTRs), and a second scale factor SC2 to allow for a different scale between the integer and fractional rods.

The best fit values were $d_1 = 0.57$, $occ_1 = 0.88$ and $SC2 = 0.58$. The value of $d_1 = 0.57$ means that the Ta atoms of the TaO have traveled 57% of the distance that separated them from the nearest site of the Ta lattice. The best-fit structure is represented in Fig. 5b.

The theoretical structure factors obtained with this model are compared to the experimental ones in Fig. 2. In contrast with a simple layer of pseudo-hexagonal KS TaO, this model gives, as desired, the correct spacing between the CTRs and the main superstructure peak, not only on the "A" and "B" lines, but also on the "C" line, which contains the (2 2) CTR.

With this model, the fit along the Ta CTRs (lines in Fig. 3) has approximately the same quality ($\chi^2 = 1.5$) as the fit obtained with the simple (1×1) model when taking into account only the atoms displaced by $(1/4, 1/4)$ from the bulk positions. The rms roughness of the Ta surface is 3.5 Å ($\beta = 0.255$) and the L-shift is -0.045.

Further improvement of the fit (especially on the CTRs) could be obtained by introducing z-displacements of a few Ta atoms. However, this had limited interest because the number of points measured on the superstructure rods was too small to obtain a description of the "buckling" of the TaO, i.e. how the z-displacements are distributed over the (5×7) supercell.

Let us now return to the comparison between the calculated and experimental reconstruction patterns. As can be seen in Fig. 2, the present "KS" model fails to reproduce the intense reconstruction peaks located at $(H_{CTR}, K_{CTR} - 1/7)$ and also the weaker ones at $(H_{CTR} - 1/5, K_{CTR} + 1/7)$. Since the superstructure peaks at $(H_{CTR}, K_{CTR} - 1/7)$ (NW peaks, this denomination is explained later) are almost as intense as the ones at $(H_{CTR} + 1/5, K_{CTR} - 2/7)$ (KS peaks), not reproducing them can seem a major failure of the "KS" model. We consider however that this failure is not crucial, because the NW peaks are a less general feature than the KS peaks.

The NW peaks are less general, because they were found on only one sample (the first one) while the KS peaks were present on all the samples (see Section 3.2). By watching the time evolution of the two types of peaks, we could conclude that the NW and KS peaks arise from two separate reconstructions on the surface: indeed, after a long stay in vacuum (six months), the NW peaks disappeared while the KS peaks remained. This time evolution also shows that the NW reconstruction is less stable than the KS reconstruction.

The "KS" model, although it does not reproduce all the peaks of the (5×7) diffraction pattern, is therefore considered as relevant, because it can be reapplied to the other samples (as will be discussed in Section 4), while a more detailed model would hold only for the (5×7) sample.

Getting a more detailed model of the (5×7) reconstruction is relatively straightforward. We

take as a starting hypothesis that the NW and KS peaks arise from two separate reconstructions. The NW reconstruction can be simplified as a (1×7), since the NW peaks are at integer values of H. The NW peaks can be approximately reproduced by considering simply a 1D misfit dislocation network along the $[1\,-1\,0]_{Ta}$ direction (i.e. the y direction), with one missing TaO atom each seven Ta sites. The name "NW" stems from the fact that this model can be built by deforming a layer of TaO(1 1 1) in NW epitaxy, in the same way that the "KS" model was built from TaO in KS epitaxy.

The link between the presence of the NW peaks in the diffraction pattern and having NW TaO on the surface is however less straightforward than the link between the KS peaks and the KS TaO: the needed deformation is more severe and the axes of this deformation are not particularly favorable in bulk Ta. The only real support for linking the NW peaks to NW TaO is the observation of TaO(1 1 1) in NW epitaxy on Ta(1 1 0) in the study of Boggio et al. [15,16].

A model with a 50–50% incoherent mixture of the KS and NW reconstructions enables to decrease the χ^2 by a factor of approximately 2 for the in-plane diffraction pattern of the (5×7). This does however not reproduce the weaker peaks at $(H_{CTR} - 1/5, K_{CTR} + 1/7)$. A possible way to obtain these latter peaks would be through a coherent tiling of the two reconstructions on the surface, but this was not tested.

3.1.2.4. Summary. To summarize this part on the atomic structure of the (5×7) reconstruction, we find that only the last Ta plane is reconstructed. It has a structure close to that of TaO(1 1 1) in KS epitaxy, deformed in a big coincidence supercell to better match the Ta lattice. The reconstruction is highly anisotropic, with a P2 symmetry, instead of P2mm for the non-reconstructed Ta(1 1 0) surface. Only the domain corresponding to displacements of the Ta atoms along the c axis of the sapphire is present.

Secondary features of the model are: (1) the presence of domains of another reconstruction which can be described as a 1D misfit dislocation network along $[1\,-1\,0]_{Ta}$. This second reconstruction could be related to the presence of TaO(1 1 1) in NW epitaxy. This feature is considered as secondary since it was observed on only one sample; (2) a possible buckling of the Ta layer.

3.2. Influence of the Ta layer thickness

As mentioned before, the (5×7) multiplicity of the reconstruction is not systematic. In this section, we develop this point in more detail.

We report here data obtained on three other samples that were grown to evaluate the effect of the Ta layer thickness on the surface reconstruction. Since the reconstruction is quite sensitive to the growth conditions, particular care was taken to ensure that the thickness was the only parameter varied between the samples (300, 1000 and 3800 Å). The three samples were grown at the same substrate temperature (900°C), the same deposition rate (0.4 Å/s), on sapphire (1 1 −2 0) substrates coming from the same wafer (miscut 1.9°, line of biggest slope along the $[-1\,1\,0\,0]$ Al_2O_3 axis) and prepared with the same procedure. Unfortunately, the three samples could not be grown out of the same Ta charge in the evaporator, 3000–4000 Å of Ta being the maximum thickness that can be grown with a single charge.

3.2.1. Diffraction patterns

Reconstruction patterns resembling the (5×7) already described were obtained on all three samples, as evidenced by RHEED and by the SXRD mesh scans. Since most of the superstructure peaks were not located along lines joining the integer rods, big mesh scans in H and K at constant L ($L = 0.3$ and 0.8) had again to be used to locate them.

As for the (5×7) sample, the main superstructure peak around the $(1\,1\,L)$ rod is located at $(H, K) = (1 + \Delta H,\ 1 + \Delta K)$, where $\Delta H > 0$ and $\Delta K < 0$, and ΔH and ΔK vary with the Ta thickness. Fig. 6a shows, for the different samples, the shift $(\Delta H, \Delta K)$ of the main superstructure peaks from the neighboring Ta CTR. These values were deduced from the in-plane mesh scans at $L = 0.3$ and 0.8 performed around different Ta CTRs, which all presented the same spacing between the CTRs and the neighboring superstructure rods

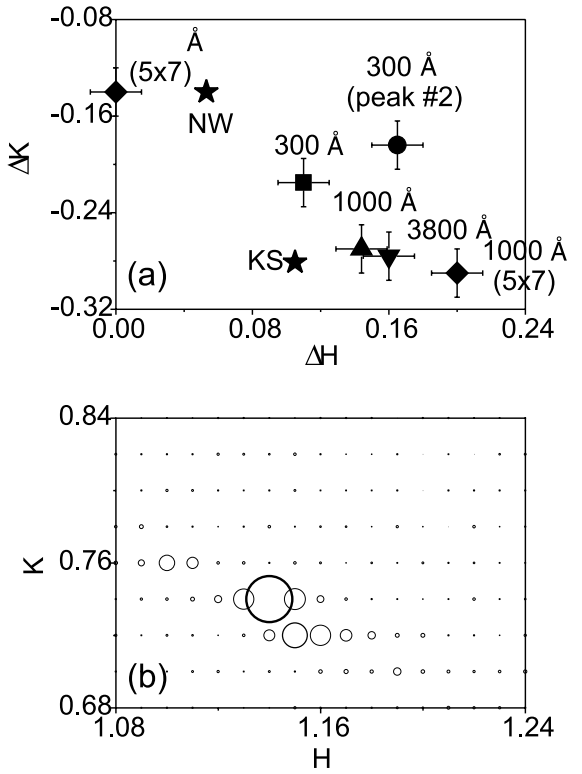

Fig. 6. (a) Average shift in H and K of the main superstructure peak(s) with respect to the Ta CTRs, for the four different samples. The positions of the TaO Bragg peaks for the KS and NW epitaxy are also indicated (★). (b) Mesh scan showing the elongation of the main superstructure peak, for the 1000 Å sample. The circle size at a given (H, K) is proportional to the intensity ($L = 0.3$).

(within the experimental uncertainties due to small misalignments). The furthest Ta CTR around which data were collected was the (2 2).

As was already discussed, the new samples do not show the superstructure peaks shifted by $(\Delta H, \Delta K) = (0, -1/n)$ from the integer rods, that were observed for the (5×7) sample. We interpreted that by attributing these peaks to a second reconstruction, which is absent on the new samples. Another remark is that the new 1000 Å-thick sample shows a reconstruction which is not (5×7). This could be due to the two times faster deposition rate used for the new sample (0.4 Å/s instead of 0.2 Å/s).

The effect of the Ta thickness on the reconstruction, as deduced from the mesh scans at $L = 0.3$ and 0.8, can be summarized as follows. When the Ta thickness decreases:

(i) the number of planes involved in the reconstruction increases: the superstructure rods, which are always parallel to the Ta CTRs, have a less flat profile along L. They peak around the same L as the neighboring Ta CTR;

(ii) the main superstructure peak moves toward the neighboring Ta CTR (see Fig. 6a);

(iii) the second domain of the reconstruction, which is absent at high thickness, reappears at low thickness: the superstructure peak at $(1 + \Delta H, -1 - \Delta K, 0.3)$ becomes more intense.

With respect to these three points, the 1000 Å sample grown with the lower deposition rate ((5×7) sample) is out of the series.

Another remarkable feature, that was found for the new 1000 and 3800 Å samples, is an elongation of the main superstructure peak along a direction roughly parallel to the $K = -0.75H$ direction. This can be seen in Fig. 6b, which shows a 2D plot of the intensity around the main superstructure peak for the 1000 Å sample. The interesting point is that the elongation takes place approximately in the direction along which the superstructure peak travels when going from one sample to another. This suggests that the two phenomena (elongation and variation of the superstructure peak position with the Ta thickness) could involve the same kind of structural defect. A possible interpretation could be that different degrees of shear coexist in a given sample, and that the average degree of shear varies with the thickness of the sample.

3.2.2. Residual strains in the Ta

As mentioned before, one of the two domains of the reconstruction is predominant in all the samples, and this domain has a fixed orientation with respect to the sapphire substrate. This is a strong indication that the underlying sapphire influences the structure of the Ta surface. One way it could influence it is through an anisotropic strain in the Ta, induced by the epitaxial stresses at the Ta/Al_2O_3 interface.

Precise bulk diffraction measurements were therefore performed in order to determine if an

Table 1
Measurements of the residual strains in the Ta for the different samples, performed at NSLS or with the X'Pert diffractometer

Sample	Thickness Å	Apparatus	(HHL)	α (%)
1 (5×7)	1000	NSLS	331	+0.17
		X'Pert	111	+0.16
2	300	NSLS	331	+0.18
3	1000	X'Pert	111	+0.13
4	3800	X'Pert	111	+0.07

The anisotropy is calculated by the formula: $\alpha = [d(H-HL)/d(HHL)] - 1$, where $d(HKL)$ is the measured inter-planes distance for plane (HKL) (surface Miller indexes). The experimental uncertainties are about ±15%.

in-plane anisotropy of the lattice parameter was present in the Ta. A small anisotropy, quantified by the ratio between the interplanar distances $d(HHL)$ and $d(H-HL)$, was found for all the samples. The results for the different samples are summarized in Table 1, which indicates the value of the in-plane anisotropy, and the type of reflections used.

Fig. 7 shows as an example the "θ–2θ" in-plane scans that were performed around the four {3 3 1} Ta Bragg peaks of the (5×7) sample. The anisotropy between the $H=K$ and $H=-K$ directions is clearly visible on this figure. The inset of Fig. 7 recalls the respective orientations of the

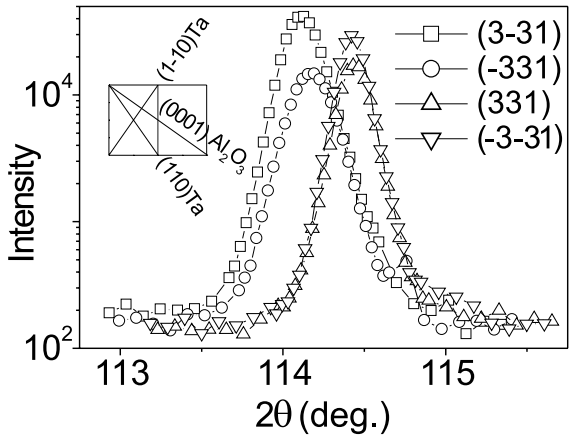

Fig. 7. The "θ–2θ" in-plane scans around the four $(HKL) = (\pm3\,\pm3\,1)$ Bragg peaks of the Ta (first sample). The anisotropy of the lattice parameter between the $H=K$ and $H=-K$ directions is clearly visible.

$(HH0)$ and $(H-H0)$ Ta planes and the sapphire (0 0 0 1) axis.

As indicated by Table 1, the anisotropy tends to decrease somewhat as the Ta thickness increases, which is the expected trend: the strain decreases as the Ta becomes more "bulk like". This tendency is however not so clear between the 300 and 1000 Å samples. This could be due to the fact that the 300 Å deposit is discontinuous, while the 1000 Å films are continuous, as indicated by the growth studies performed by Ritley et al. [23].

For the 300 Å sample, the absolute values of the residual strains in the $H=K$ and $H=-K$ directions were also measured at NSLS. They were obtained by comparing the positions of the Ta Bragg peaks to those of "reference" neighboring sapphire Bragg peaks. The reference lattice parameters used here were $a = 3.3058$ Å for Ta and $a = 4.7587$ Å, $c = 12.9929$ Å for sapphire. The absolute strain measurements show that the Ta is within 0.03% of its bulk lattice parameter for the (1 −1 1) planes, that are parallel to the sapphire (0 0 0 1) axis, and that there is a 0.2% contraction of the distance between the (1 1 1) planes, that are 19.5° off the perpendicular to the sapphire (0 0 0 1) axis. By reaction to this "bulk" strain in the Ta, one would expect the surface structure to show an expansion of the (1 1 1) inter-plane distance, and more generally to involve displacements along the $[1\,-1\,2]_{Ta}$ direction. This is reasonably consistent with the experimental tendency that the preferred domain is the one involving a shear of the Ta along the $[1\,-1\,1]_{Ta}$ direction, while the one involving a shear along the $[-1\,1\,1]_{Ta}$ direction is almost absent.

4. Discussion

4.1. Nature of the reconstruction

Since Lee et al. [24] concluded, in their study of Nb/Al_2O_3 thin films, that the X-ray satellites they observed were due to a misfit dislocation network at the interface, the question arises if the reconstruction seen here could enter in this category. The superstructure peaks could in principle arise

from four different situations: (i) a surface reconstruction, with atomic displacements limited to the last few planes of the Ta; (ii) a localized interface reconstruction, with atomic displacements limited to the first few planes of the Ta, closest to the sapphire; (iii) a misfit dislocation network, with atomic displacements extending over the whole thickness of the film; (iv) a facetting of the Ta surface.

Since the superstructure peaks can be seen by RHEED, and since RHEED has a very small penetration depth (maximum a few tens of Å), we can exclude option (ii), where the reconstruction does not reach the surface. A facetting (option (iv)) would give inclined superstructure rods. Here the superstructure rods are parallel to the Ta CTRs (i.e. perpendicular to the surface) so we can exclude option (iv). A misfit dislocation network (option (ii)) would give superstructure rods that are strongly peaked in L [25], since they come from a thick layer. Here the superstructure rods for the 1000 Å films have an almost flat profile along L, so we can exclude option (ii) for the thicker samples. For the 300 Å sample, the presence of a misfit dislocation network is not completely impossible, since the superstructure rods are less flat.

Our conclusion is that the superstructure peaks seen on the thicker samples arise from a surface reconstruction, which involves at most one or two Ta planes.

4.2. Atomic structure for the last three samples

For all the samples studied here, the Ta layer presents the same kind of surface reconstruction. However, the exact positions of the superstructure peaks vary. Since the atomic structure was obtained from the data taken on only one sample, one needs to check if it also describes to the other samples.

For solving the atomic structure, we chose one particular sample, whose reconstruction was (5×7). This sample was chosen because its diffraction pattern was the closest to what we could call a "conventional surface reconstruction": (1) it had several superstructure peaks close enough to each other to easily define a reconstruction unit cell in reciprocal space; (2) the corresponding supercell in direct space was a $(m \times n)$ multiple of the Ta unit cell, with relatively small m and n numbers. In other words, it was clear from the diffraction pattern that the supercell was commensurate with the Ta unit cell. This commensurate character, as well as the relatively small size of the supercell, enabled to use the standard surface diffraction analysis program (ROD) to solve the atomic structure.

During the analysis, however, it appeared that the atomic structure had not much to do with conventional reconstructions such as (1×2) or $(\sqrt{3} \times \sqrt{3})$. The pattern resembled much more the ones obtained when there is an interfacial dislocation network between two materials of small misfit. And the final structure that we proposed can in fact be described as a misfit defect network at the interface between a single TaO plane and the underlying Ta substrate.

For the new 1000 and 3800 Å samples, the diffraction pattern is even more remote than the (5×7) pattern from conventional surface reconstructions, and closer to misfit dislocation networks: there is basically only one family of superstructure peaks, at positions of the type $(H_{\mathrm{CTR}} + \Delta H, K_{\mathrm{CTR}} + \Delta K)$, with a $(\Delta H, \Delta K)$ not particularly equal to $(1/n, -2/m)$.

Since the "KS" model gives only one family of intense superstructure peaks (Fig. 2), it is compatible with the first feature of this pattern. The second feature, which is the "non-rational" character of the superstructure peaks, can be solved by considering a coherent mixture of supercells of slightly different multiplicities.

Such a mixture of supercells of slightly different sizes has already been observed on an oxidized Nb(1 1 0) single crystal [26]. The authors of Ref. [26] observed by STM prominent 30 Å long "sticks" parallel to $\langle 1\,1\,1 \rangle_{\mathrm{Nb}}$, with a variable spacing of 3, 4, or 5 $(-1\,1\,2)_{\mathrm{Ta}}$ distances. A mixture of periods is also physically compatible with the proposed "misfit defect" model. Indeed, interfacial misfit dislocation networks typically produce a random mixture of supercells of slightly different periods, because the matching between n substrate lattice units and m adsorbate lattice units is never perfect.

To summarize, it seems reasonable to propose that the pattern observed on the new 1000 and 3800 Å samples results from the coexistence of supercells of slightly different sizes along $[-1\,1\,2]_{Ta}$. Each supercell would contain deformed KS TaO with a slightly different degree of shear. The coherent scattering between the supercells of different sizes would produce $(\Delta H, \Delta K)$ values that are not exactly of the form $(1/n, -2/m)$, as well as an elongation of the peaks.

4.3. Domain selection

In all the samples, we observed a predominance, complete or partial, of the first domain of the reconstruction (main superstructure peak at $(1+\Delta H, 1+\Delta K)$) with respect to the second domain (main superstructure peak at $(1+\Delta H, -1-\Delta K)$). We attributed this predominance to the fact that the surface shear along $[1\,-1\,1]_{Ta}$ relieves the anisotropic stress in the Ta caused by the sapphire.

Further support to this interpretation is brought by the literature. Swiech et al. [2] demonstrated for Nb/Al_2O_3 the possibility to make the second domain reappear by heating the sample between 1100°C and 1210°C. In contrast, Pantel et al. [3] found that the same kind of reconstruction on a Nb(1 1 0) single crystal was stable up to 2000°C. It seems quite clear that the effect observed by Swiech et al. [2] comes from a thermal variation in the strain of the Nb induced by the sapphire, not present for a Nb single crystal. This variation could be driven by a variation of misfit at the Nb/Al_2O_3 interface, induced either by the small difference of thermal expansion between Nb and Al_2O_3, or by the anisotropic thermal expansion of the sapphire. The Nb/Al_2O_3 system is known to have very small misfit variations with the temperature [5,27], from −11.84% and −1.73% at room temperature to −11.98% and −1.8% at 1200°C. However, only small variations would be necessary to make the period of the dislocation network exactly match an integer number of Nb and Al_2O_3 lattice spacings, leading to a removal of the residual strain.

When comparing the different samples, no particular correlation appears between the amount of second domain and the value of the strain anisotropy. What matters in the choice of the domain is apparently not the average strain anisotropy in the Ta, but the way the strain is distributed across the surface. The study of Nb/Al_2O_3 by Swiech et al. [2] tends to indicate that the second domain is present only in defective regions of the surface, where the strain field is perturbed. This could explain why there is a large amount of second domain in the 300 Å sample: this deposit, with its 3D morphology and small thickness, is likely to present a very inhomogeneous strain field.

Another hypothesis would be that the domain selection comes from the presence of parallel steps on the Ta surface, related to the large miscut of our sapphire crystals (1.1–1.9°). This hypothesis can however not be used to explain the experiments of Swiech et al., which were done using sapphire of very small miscut (<0.1°).

4.4. Period of the reconstruction

We examine here which factors are likely to determine the period of the reconstruction. As discussed in Section 4.2, it is likely that several supercells of slightly different periods coexist on the surface. What we will discuss here is therefore only the average period.

A first factor that can influence the periodicity of the reconstruction is the oxygen concentration at the surface. It is clear, by analogy with the study of Pantel et al. [3] on Nb, that the reconstruction observed here is due to oxygen. However, it was not possible to measure the amount of oxygen present on the surface of the different samples, because charging effects prevented the analysis by Auger electron spectroscopy.

A second factor that can influence the periodicity of the reconstruction is the amount of residual strains in the bulk of the Ta. Some support to this hypothesis is brought by the observation of Swiech et al. [2] that the positions of the superstructure peaks vary with the temperature of the Nb/Al_2O_3 sample. Our data concerning the last three samples indicate a shift of the superstructure away from the Ta CTR as the strain anisotropy in the Ta decreases. This tendency is however not conserved when considering the sample grown with a lower deposition rate (first sample).

These data indicate that the average period of the reconstruction depends on a combination of several factors, including most likely the strain in the Ta and the oxygen concentration. Auger analysis and absolute strain measurements would be necessary to disentangle the respective effects of the different factors.

5. Conclusion

The atomic structure of the Ta reconstruction has been partially solved. The reconstruction can be described as a misfit defect network at the interface between one plane of TaO(1 1 1) in KS epitaxy and the Ta. The model is build by first deforming the KS TaO to obtain the coincidence supercell with the Ta, and secondly moving the Ta atoms of the TaO toward the nearest adsorption sites of the underlying Ta. The reconstruction is not always commensurate. This has been interpreted as due to the coexistence of several commensurate supercells of slightly different periods. A small anisotropy (0.1–0.2%) of the in-plane lattice parameter of the Ta has been detected in all the samples. This anisotropy, which is due to the epitaxy on the sapphire, induces on the surface a selection of one of the two domains of the reconstruction. The average period of the reconstruction is very sensitive to the growth conditions. Measurements of the surface oxygen concentration and of the absolute film strain would be necessary to understand the mechanism that determines this period.

Acknowledgements

We acknowledge the support of the US Department of Energy through grant number DEFG02-96ER45439. The NSLS is supported by the DOE under program DEAC02-98CH10886.

References

[1] JCPDS database 1997.
[2] W. Swiech, R.S. Appleton, B.D. Wiemeyer, C.P. Flynn, Surf. Rev. Lett. 5 (6) (1998) 1221.
[3] R. Pantel, M. Bujor, J. Bardolle, Surf. Sci. 62 (1977) 589.
[4] S.M. Durbin, J.E. Cunningham, C.P. Flynn, J. Phys. F: Met. Phys. 12 (1982) L75.
[5] G. Gutekunst, J. Mayer, M. Rühle, Phil. Mag. A 75 (5) (1997) 1329.
[6] G. Gutekunst, J. Mayer, V. Vitek, M. Rühle, Phil. Mag. A 75 (5) (1997) 1357.
[7] K.A. Ritley, Growth and magnetoelastic behavior of *b*-axis oriented dysprosium, Ph.D. Thesis, University of Illinois at Urbana-Champaign, 1998.
[8] K.L. Whiteaker, Compositional order and structure of epitaxial thin film semiconductors by X-ray diffraction, Ph.D. Thesis, University of Illinois at Urbana-Champaign, 1997.
[9] X. Wang, U. Helmersson, J. Birch, W. Ni, J. Cryst. Growth 171 (1997) 401.
[10] I.K. Robinson, Phys. Rev. B 33 (6) (1986) 3830.
[11] S.R. Andrews, R.A. Cowley, J. Phys. C 18 (1985) 6427.
[12] E. Vlieg, J. Appl. Cryst. 33 (2000) 401.
[13] http://www.esrf.fr/computing/scientific/joint_projects/ANA-ROD/index.html.
[14] B.E. Warren, X-ray Diffraction, Dover, New York, 1990.
[15] J.E. Boggio, H.E. Farnsworth, Surf. Sci. 1 (1964) 399.
[16] J.E. Boggio, H.E. Farnsworth, Surf. Sci. 3 (1964) 62.
[17] R. Franchy, T.U. Barke, P. Gassman, Surf. Sci. 366 (1996) 60.
[18] K.H. Rieder, Appl. Surf. Sci. 4 (1980) 183.
[19] O. Hellwig, J. Heise, M. Ay, H. Zabel, Annual report 1998, Ruhr Universität, Bochum.
[20] T.W. Haas, A.G. Jackson, M.P. Hooker, J. Chem. Phys. 46 (8) (1967) 3025.
[21] C. Sürgers, H.v. Löhneysen, Appl. Phys. A 54 (1992) 350.
[22] A. Zangwill, Physics at Surfaces, Cambridge University Press, Cambridge, 1988.
[23] K.A. Ritley, C.S. Durfee, private communication.
[24] C.H. Lee, K.S. Liang, F.S. Shieu, S.L. Sass, C.P. Flynn, Mater. Res. Soc. Symp. Proc. 209 (1991) 679.
[25] G. Renaud, private communication.
[26] I. Arfaoui, J. Cousty, H. Safa, ECOSS 19th Abstracts booklet, Madrid, 2000, p. 87.
[27] D.E. Gray (Ed.), American Institute of Physics Handbook, McGraw-Hill, New York, 1972.